Proceedings of the ASME 2010 3rd Joint US-European Fluids Engineering Summer Meeting and 8th International Conference on Nanochannels, Microchannels, and Minichannels
FEDSM-ICNMM2010
August 1-5, 2010, Montreal, Canada

FEDSM-ICNMM2010-30393

EXPERIMENTAL AND NUMERICAL INVESTIGATIONS OF A TRANSONIC, HIGH TURNING TURBINE CASCADE WITH A DIVERGENT ENDWALL

Santosh Abraham, Kapil Panchal, Song Xue, Srinath V Ekkad, Wing Ng
Department of Mechanical Engineering, Virginia Tech
Blacksburg, VA, USA

Barry J. Brown
Florida Turbine Technologies, Inc.
Jupiter, Fl, USA

Anthony Malandra
Siemens
Orlando, Fl, USA

ABSTRACT

The paper presents detailed measurements of midspan total pressure loss, secondary flow field, static pressure measurements on airfoil surface at midspan, near hub and near the end walls in a transonic turbine airfoil cascade. Numerous low-speed experimental studies have been carried out to investigate the performance of turbine cascades. Profile and secondary loss correlations have been developed and improved over the years to include the induced incidence and leading edge geometry and to reflect recent trends in turbine design. All of the above investigations have resulted in better understanding of flow field in turbine passages. However, there is still insufficient data on the performance of turbine blades with high turning angles operating at varying incidences angles at transonic Mach numbers. In the present study, measurements were made at +10, 0 and -10 degree incidence angles for a high turning turbine airfoil with 127 degree turning. The exit Mach numbers were varied within a range from 0.6 to 1.1. Additionally, the exit span is increased relative to the inlet span resulting in one end wall diverging from inlet to exit at 13 degree angle. This was done in order to obtain a ratio of inlet Mach number to exit Mach number which is representative to that encountered in real engine and simulates the blade and near end wall loading that is seen in an engine. 3D viscous compressible CFD analysis was carried out in order to compare the results with experimentally obtained values and to further investigate the design and off-design flow characteristics of the airfoil under study. All aerodynamic measurements were compared with CFD analysis and a reasonably good match was observed.

INTRODUCTION

With present day stringent norms set by the government for clean and efficient engines and the ever-growing competition in the market, gas turbine manufactures need to optimize every component of the engine. The need for low cost, compact and fuel efficient engines are apparent. Improvements can be made by designing blades such that minimum losses are generated while making sure that the loading on the blade is maximized in order to reduce the number of airfoils in each stage. The designer also needs to ensure that the turbine efficiency is maintained at off-design conditions. Almost a third of the total losses in turbines are due to end wall losses. The thickness of the upstream boundary layer as well as the blade turning angle influences the strength of the secondary flow observed near the end walls. The secondary flow results into stagnation pressure loss which accounts for a considerable portion of the total stagnation pressure loss occurring in a turbine passage.

Various investigations have been conducted in linear turbine cascades to optimize the design of blades. Most of the previous studies have been conducted at subsonic flow conditions [1–3]. Recent work by Prakash et al. [4] studied the profile losses and loading at the midspan. The works of Popovic et al. [5], and Zoric et al. [6, 7] revealed high profile loss for aft loaded blades and high secondary losses for front loaded blades. However there is less information on the performance of blades at transonic flow conditions with high turning angles operating at varying incidences as is investigated in this study. Jouini et al. [8, 9] investigated the flow field for transonic linear turbine cascades at design and off-design conditions. Notable recent

efforts in computational fluid dynamics codes involve the work of Praisner and Clark [10, 11] and Menter et al. [12, 13]. Many researchers have previously used quasi-linear cascade design with divergent end walls, similar to the one used in the present study, in order to achieve loading distribution similar to that of a real engine. A similar quasi 2D cascade was used by Nagel et al. [14] with the same goal in mind.

The following sections discuss experimental setup, CFD analysis and aerodynamic measurements from experiments and CFD analysis for a transonic linear cascade with a high turning angle turbine blade at both design as well as off-design conditions.

NOMENCLATURE

C_{ax}	Blade Axial Chord Length
M	Isentropic Mach Number $= \sqrt{\left[\left(\frac{p_{01}}{p_{s2}}\right)^{\frac{\gamma-1}{\gamma}} - 1\right]\frac{2}{\gamma-1}}$
p_{01}	Inlet Total Pressure measured 0.45 C_{ax} upstream of the cascade
p_{02}	Exit Total Pressure
p_{s2}	Exit Static Pressure
PS	Pressure Surface
SS	Suction Surface
x	Axial Coordinate
ω	Loss coefficient $= \frac{p_{01}-p_{02}}{p_{01}-p_{s2}}$

DESCRIPTION OF THE FACILITY

The two-dimensional Virginia Tech transonic cascade wind tunnel shown in Figure 1 is a blow down facility that is capable of sustaining a constant inlet pressure in the test section for up to 20 seconds. Air is supplied from high pressure air tanks that are charged up to 2068 kPa (300psig) prior to testing. A control valve regulates the flow from the air tanks to the test section.

The cascade, as shown in Figure 2, consists of 6 blades resulting in 5 passages. Blade 3 is considered as the center blade and has been instrumented to measure the static pressure at mid span. The blades above(blade 2) and below(blade 4) the center blade are instrumented on the pressure side and suction side respectively for midspan static pressure measurement to ensure flow periodicity in two adjacent passages around the center blade 3. Tailboards are positioned at the top and bottom blade trailing edges to help aid in creating a periodic flow through the cascade. A headboard, positioned upstream of the cascade is instrumental in controlling the incoming flow by preventing an induced incidence angle effect on the leading edges of the blades. The headboard is used to create and control a flow bleed that prevents the flow from turning prior to reaching the leading edge of the blades. This aids in maintaining uniform and periodic flow through each blade passage. A slot located 0.45 C_{ax} upstream of the cascade is used to measure the turbulence and velocity distribution at the inlet of the cascade. It is also used to measure inlet total pressure at midspan which is used as a reference total pressure for isentropic Mach number calculation.

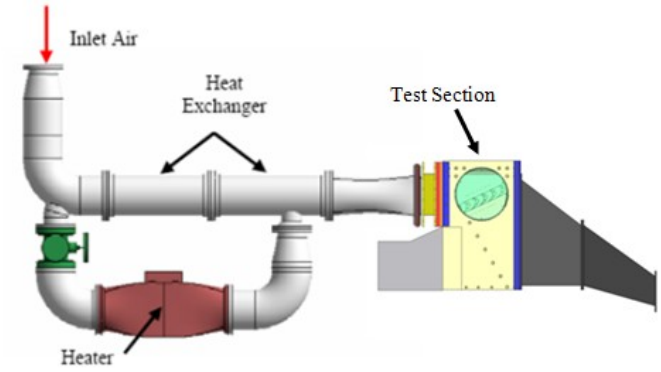

Figure 1 : Virginia Tech transonic cascade wind tunnel

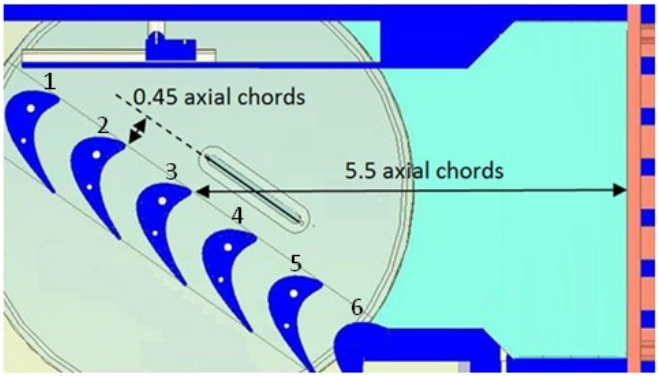

Figure 2 : Cascade diagram showing the blades and the axis orientation for measurements with the traverse

The blade span increases by about 16% linearly in axial direction from inlet to exit of the cascade as shown in Figure 3 on the next page. This expansion has been incorporated into the design to obtain a ratio of inlet/exit Mach number representative of a real engine and simulates the end wall loading that is seen in an engine.

MEASUREMENT TECHNIQUES

Inlet Flow Measurements

Aerodynamic measurements were made on a plane 0. 45 C_{ax} upstream of the blade leading edge. The turbulence grid was located 5.5 C_{ax} upstream as shown in Figure 2. The measurements covered one and a half blade pitches and extended from near the end wall to the midspan. A pitot probe was used to measure the inlet velocities at midspan and also to estimate the boundary layer thickness. Uniformity of the incoming flow was established by pitchwise traverse measurements. A single line hot-wire probe was employed to measure the inlet free stream turbulence intensity based on isotropic turbulence assumption.

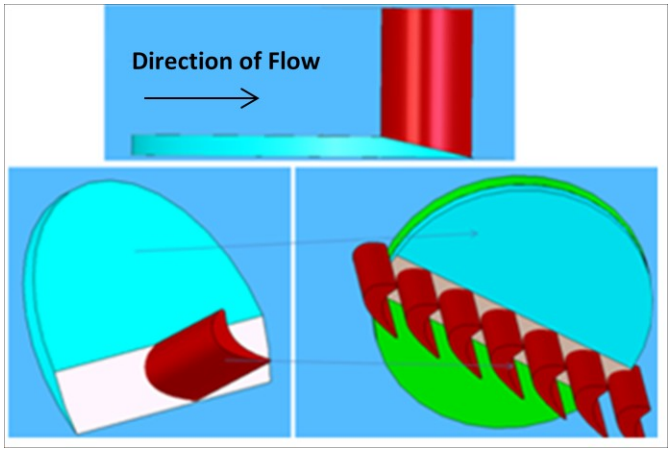

Figure 3 : Change in inlet span relative to exit span

Static Pressure Measurements

To calculate the local isentropic blade surface Mach number, the center blade and two adjacent blades were instrumented with total 60 pressure taps places at the midspan. Static pressure taps were positioned on the end walls of the cascade on a plane 0.5 C_{ax} upstream of the blade leading edges and 0.5 C_{ax} downstream of the blade trailing edges in order to estimate the inlet and exit Mach numbers. The exit static pressure measurements are also used to calculate the loss coefficient.

Loss coefficient measurements 0.1 and 1.0 axial chord downstream

The loss coefficient measurements were carried out at both 0.1 as well as 1.0 axial chord downstream from the blade trailing edge. A 5-hole probe was used to capture the velocity profiles in both the spanwise as well as in the pitchwise direction. The pitchwise area averaged loss coefficient was measured at midspan for mach numbers varying from 0.6 to 1.1 and for incidence angles -10, 0 and +10. The spanwise area averaged loss coefficient was measured at 6 different spanwise locations for the design exit Mach number and the design incidence angle.

CFD ANALYSIS

Three dimensional viscous compressible computational fluid dynamic analysis was carried out for the blade and the blade surface mid-span measurements were compared with experimental results in order to validate the results of CFD analysis. Once validated, this analysis was used to further investigate the flow in the blade passage under study.

Computational Geometry and Grid

Figure 4 shows the computational domain used for the analysis. The domain consist of a blade with two periodic sides at half pitch distance from axial leading edge on both the sides of the blade extended 0.5 C_{ax} upstream and 1.5 C_{ax} downstream of the cascade in axial direction. The blade has one angled end wall diverging from inlet to exit flat end wall as in the experimental setup. Hence, one passage of the turbine blade linear cascade has been modeled here.

The grid shown in Figure 4 was selected after a grid sensitivity test. Details of the grid sensitivity test are given in ensuing discussion. The unstructured grid used here consists of prismatic cell inflation layers near blade and end wall surfaces to effectively model the flow within the boundary layer. A zoomed in section of the grid is shown in Figure 4 which shows such inflation layer bunching near one of the end walls. Inflation layer is a layer of prismatic cells which can simulate near wall physics more effectively than tetrahedron shape cells used for unstructured grid.

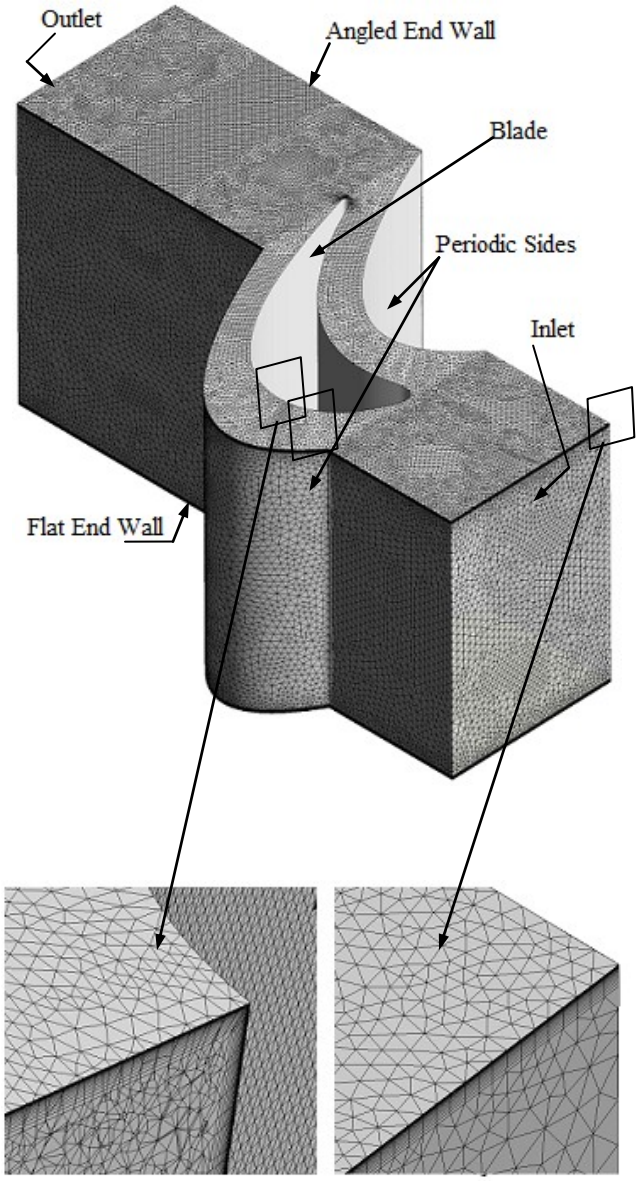

Figure 4 : Top - Computational Mesh With Boundary Conditions, Bottom - Zoomed in Mesh Showing Prismatic Inflation Layers

Computational Model and Boundary Conditions

Various boundary conditions applied on the model are as shown in Figure 4. Inlet total pressure and total temperature are specified at the inlet along with the designed inlet flow

direction. The mass flow angle 4mm in front of the blade axial leading edge is considered as design flow angle. In order to achieve design flow angle at this location, the flow direction at inlet was specified with 3.25 degree positive incidence angle. The total pressure profile within the boundary layer and a constant total pressure elsewhere was specified at the inlet boundary using the experimentally measured values.

A prescribed average static pressure condition was specified at the outlet boundaries. Side walls were given translational periodicity boundary condition. The end walls and the blade surface were specified to be adiabatic walls with zero slip.

SST-k ω turbulence model was used based on past experience with similar aerodynamic simulations with flows over turbine blades. Convergence criteria form RMS residuals was chosen to be 5×10^{-5}. The CFD solver produced blade loading and loss coefficient results that are in reasonably well agreement with the experimental results as discussed in the 'Results' section and hence the code is considered validated.

Grid Sensitivity Test

Six different grids as described in Table 1 were used for grid sensitivity test. Different combinations of body spacing, blade and end wall face spacing, presence or absence of inflation layers and number of prismatic inflation layers were tried.

Table 1 : Grid sensitivity test matrix

Grid Name	Number of Nodes	Maximum body spacing (mm)	Maximum face spacing on blade and end walls (mm)	Number of prismatic inflation layers (First layer height – mm)
O	1684866	1.5	1.5	0
A	2765614	3	1	24 (0.005)
B	2685433	4	1	24 (0.005)
C	1076905	3	2	24 (0.005)
D	1660933	3	1.5	24 (0.005)
F	1478440	3	1	20 (0.005)

It was observed that for the similar number of nodes, a grid without inflation layers showed considerably (about 70 times) high y^+values as compared to the grid with prismatic inflation layers near blade and end wall surface. Also, a significant difference in blade loading was observed toward the end of the blade region between the grid with inflation layers and the grid without inflation layers, the grid with inflation layers giving better agreement with the experimental data. The remaining 5 grids with inflation layers showed almost identical mid-span blade loading.

The remaining 5 meshes were compared for inlet flow angle, maximum y^+ value, midspan blade loading, and loss coefficient 1.0 axial chord downstream of the cascade. The maximum difference was found in loss coefficient 1.0 axial chord downstream which amounts to be about 1.2% and hence considered insignificant. The grids C,E and F have similar but considerably lower number of nodes. These grids did not show any significant difference in time to reach convergence and hence the grid E with higher face spacing was chosen as the final grid for all the simulations.

RESULTS

Inlet Flow Measurements

Well-documented inlet boundary conditions are needed for CFD calculations. Aerodynamic inlet spanwise measurements on a plane 0.5 axial chord upstream of the blade leading edge plane revealed that the inlet flow had about 11 mm thick boundary layer from the end wall as shown in Figure 5. The primary measurement passage measured an isotropic turbulence intensity level of 8%. The upstream flow uniformity was established with a maximum deviation of ±0.4%. The average inlet Mach number at design condition was 0.41.

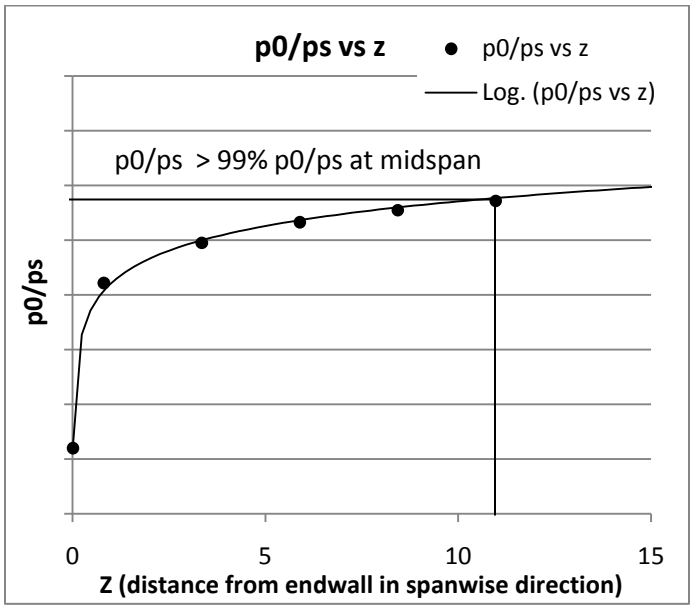

Figure 5 : (p0/ps) ratio variation normal to the end wall (z coordinate)

Static Pressure Measurements

The surface isentropic Mach number was obtained from the ratio of the measured surface static pressure at midspan to the total pressure upstream of the cascade. The uncertainty was established at ±0.1%. The local Mach number distribution on the blade surface was measured for 6 different exit Mach numbers at 3 different incidence angles. Figure 6 shows the Mach number distribution on the blade surfaces at midspan for the center 3 blades at design conditions. The periodicity of flow through the passages was satisfactory and was established for all the cases that were studied.

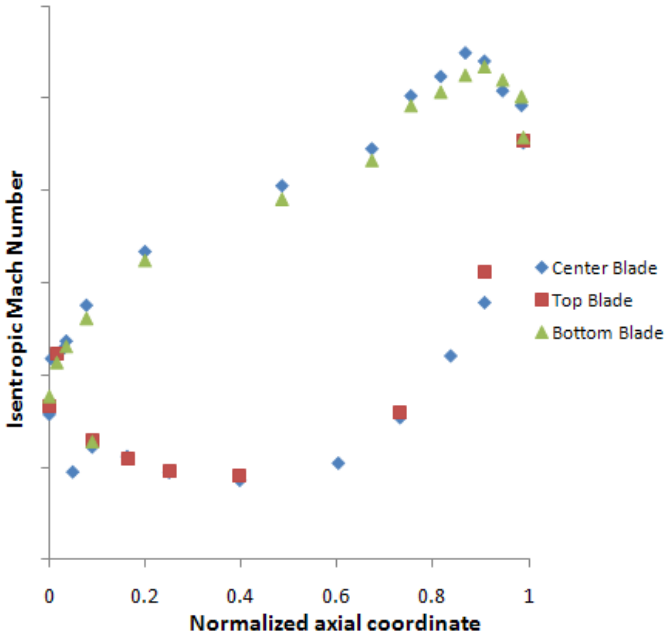

Figure 6 : Flow Periodicity in the Cascade

Figure 7 shows comparison of midspan blade loading between experimental values and CFD analysis results at 0 degree incidence and design Mach number. It can be seen that there is a very good agreement between experiments and CFD analysis. The small discrepancy observed at the axial leading edge between CFD and experiments may be attributed to the induced incidence effect due to high turning in the experiments.

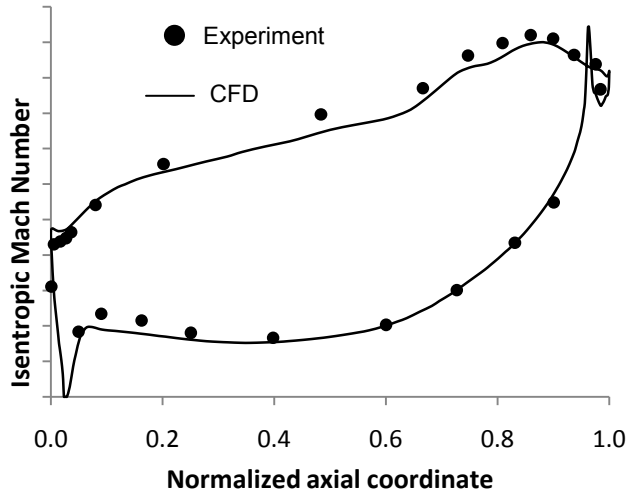

Figure 7 : Comparison of midspan blade loading from CFD analysis and experiments at design condition

The effect of variation in incidence angle can be observed from the vorticity plots for 0 degree and +10 degree incidence angles obtained from CFD analysis as shown in Figure 8 (a) and (b) respectively. Existence of large separated flow field for +10 degree incidence as compared to moderate secondary flow structure for 0 degree incidence angle suggests lower loading for +10 degree incidence angle as compared to design conditions.

The effects of the exit Mach number on the surface Mach number distribution at the design incidence angle as well as the two off-design incidence angles are shown in Figure 9 (a), (b) and (c). It is evident from the figure that the pressure side distribution does not vary significantly with the variation in exit Mach number. At lower exit Mach numbers ($M < 0.8$) the pressure surface loading remains almost constant from about 75 percent of the axial chord up to the trailing edge. At higher exit Mach numbers a normal shock impinges on the suction side and as the Mach number increases further, the shock becomes sharper and migrates more towards the trailing edge.

The effect of varying incidence angle in this case also reveals large changes in the loading distribution in the vicinity of the leading edge. As the positive incidence increases a strong suction peak develops on the suction side near the leading edge (Figure 9 (c)) and as the incidence angle reduces to -10 degrees the leading edge loading considerably decreases (Figure 9 (b)).

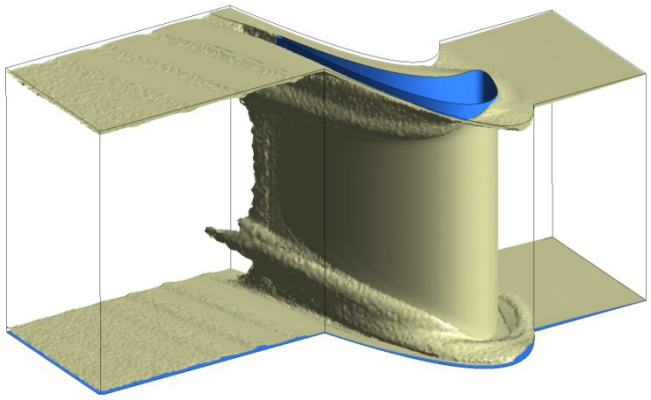

Figure 8 : (a) Vorticity Isosurface for 0 degree incidence

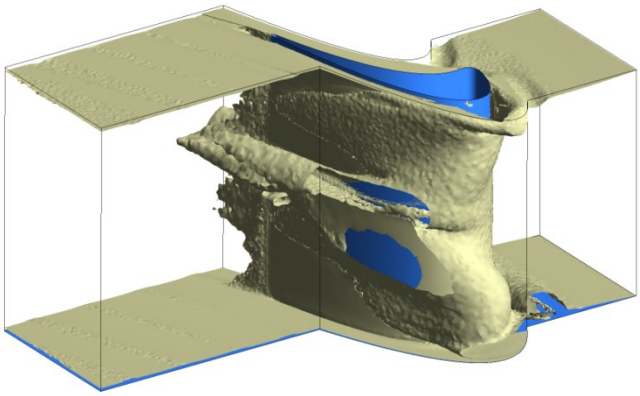

Figure 8 : (b) Vorticity Isosurface for +10 degree incidence

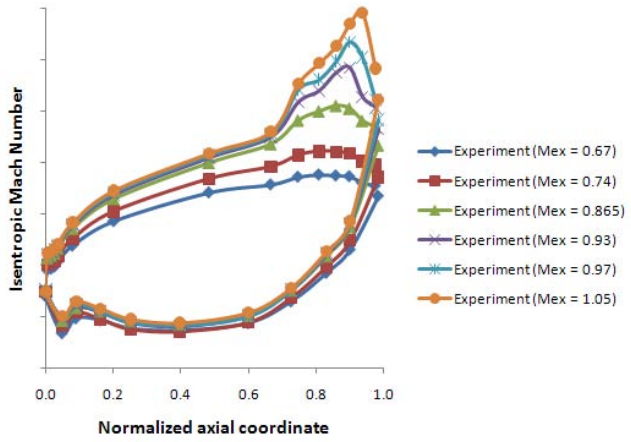

Figure 9 (a) Effects of Mach number on blade loading at design incidence

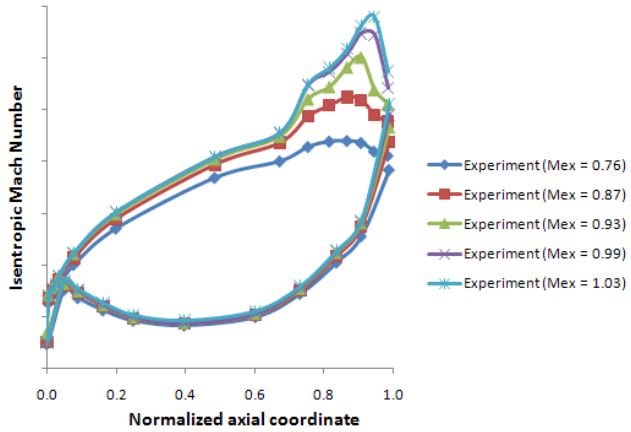

Figure 9 (b) Effects of the Mach number on blade loading at -10.0 deg off-design incidence

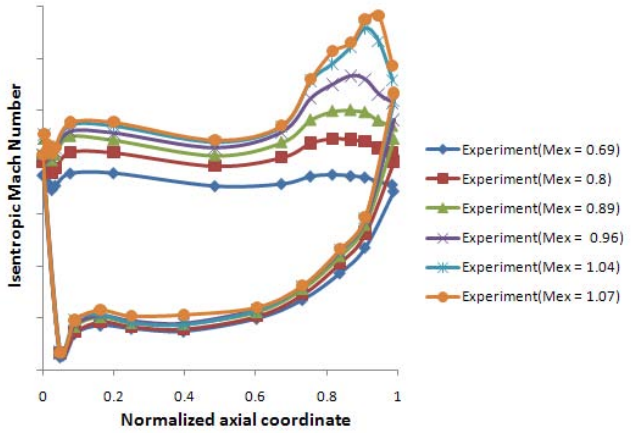

Figure 9 (c) Effects of Mach number on blade loading at +10.0 deg off-design incidence

Loss coefficient measurements 0.1 and 1.0 axial chord downstream:

Figure 10 shows a 2-D profile of the losses 0.1 axial chord downstream from the trailing edge of the cascade at the design exit Mach number and at the design incidence angle measured at various spanwise locations using a 5 hole probe. Regions of higher losses are clearly visible near the end walls and are a result of complex vortices arising due to the secondary flows. Pressure gradients in the passage caused by the boundary layer velocity distribution and flow stagnation on the blade result in the creation of secondary flows in the end wall region. These pressure variations force the flows toward the end wall and also lead to the development of two legs of the leading edge vortex. The turning angle of the flow between the airfoils results in the creation of a strong pressure gradient across the passage. This gradient influences the paths of the two legs of the horseshoe vortex and also the low velocity flow near the end wall. The pressure side leg of the horseshoe vortex which is forced to flow in a downward direction combines with the low velocity flow near the end wall and forms the passage vortex. The passage vortex drifts from the pressure side leading edge toward the suction side trailing edge of the adjacent airfoil. As this vortex approaches the suction side, it lifts off the end wall, adheres along the suction side and moves downstream in the passage. At the same time the suction side horseshoe vortex remains close to the end wall until it meets the passage vortex. It then wraps itself around the passage vortex instead of adhering to the suction surface, lifts off the end wall and continues downstream along the suction side. As we go further downstream from the trailing edge plane, these vortices mix out and at 1.0 axial chord downstream the losses are almost completely mixed out.

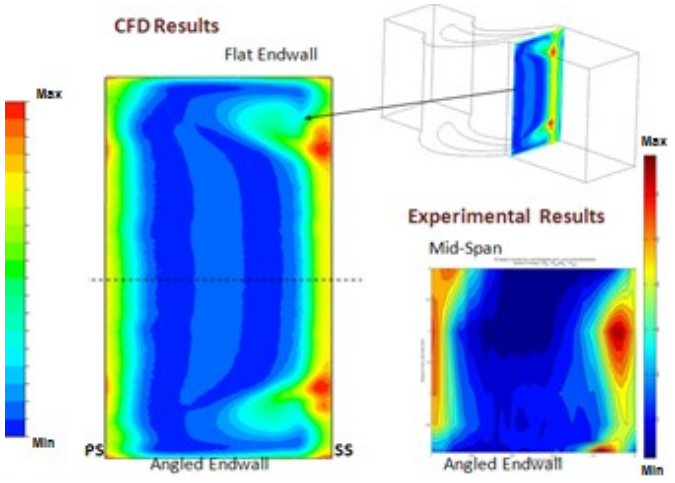

Figure 10 : Loss coefficient at 0.1 axial chord downstream

At 0.1 axial chord downstream of the trailing edge, there exists too much uncertainty due to shear layer effects. Therefore the losses are measured 1.0 axial chord downstream from the trailing edge of the cascade at different incidence angles and varying exit Mach numbers and are represented in Figure 11. For both the design incidence angle as well as the -10 degree off design incidence angle, at low exit Mach numbers the loss coefficient asymptotically reaches a limiting value. In other

words, at lower subsonic exit Mach numbers, the losses are relatively steady. However for the +10 degree case, the asymptotic behavior is not evident. The rise in losses as the exit Mach number decreases could be due to the increased loss production in the suction side boundary layer on the frontward part of the blade. This behavior at higher incidence angles was also observed by Jouini [8]. As the exit Mach number increases, the shocks become stronger and, as expected, the loss coefficient begins to rise for all incidence angles.

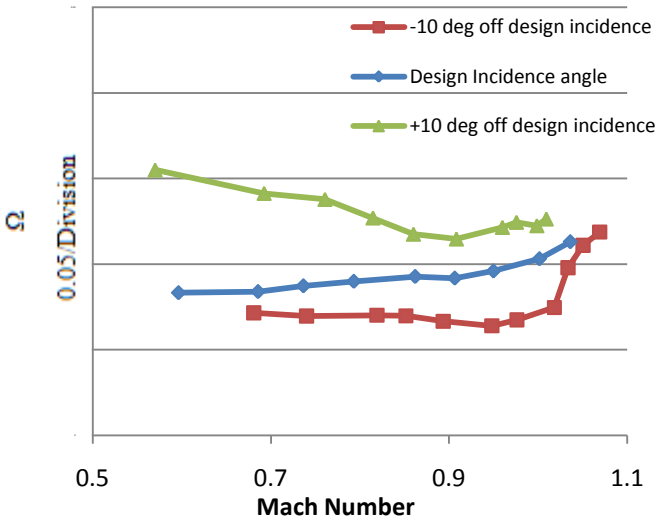

Figure 11 : Midspan average loss coefficient at 1.0 axial chord

All the loss profiles were compared with corresponding results from CFD analysis as shown in Figure 12 (a), (b) and (c) for 0 incidence angle, -10 degree incidence and +10 degree incidence respectively. A very good match between CFD predictions and experimental loss measurements were observed. However, for the +10 degree case CFD under predicted the loss values as compared to the experimental values. Sudden rise of total pressure loss at near sonic and supersonic isentropic Mach numbers as observed in experiments is also evident in CFD predictions. Experiment

CONCLUSIONS

Experimental measurements and numerical predictions for a high turning high loading turbine blade have been carried out at design and off design conditions in a linear transonic cascade wind tunnel.

The results show that at a given incidence angle, the effect of variation of exit Mach number is felt only toward the trailing edge region of blade and the loading at leading edge remains almost same for different Mach numbers. However, at off-design incidence angles the leading edge loading changes considerably reducing the overall loading in comparison to that obtained at design angle. The blade loading results from experiment and CFD analysis agree very well.

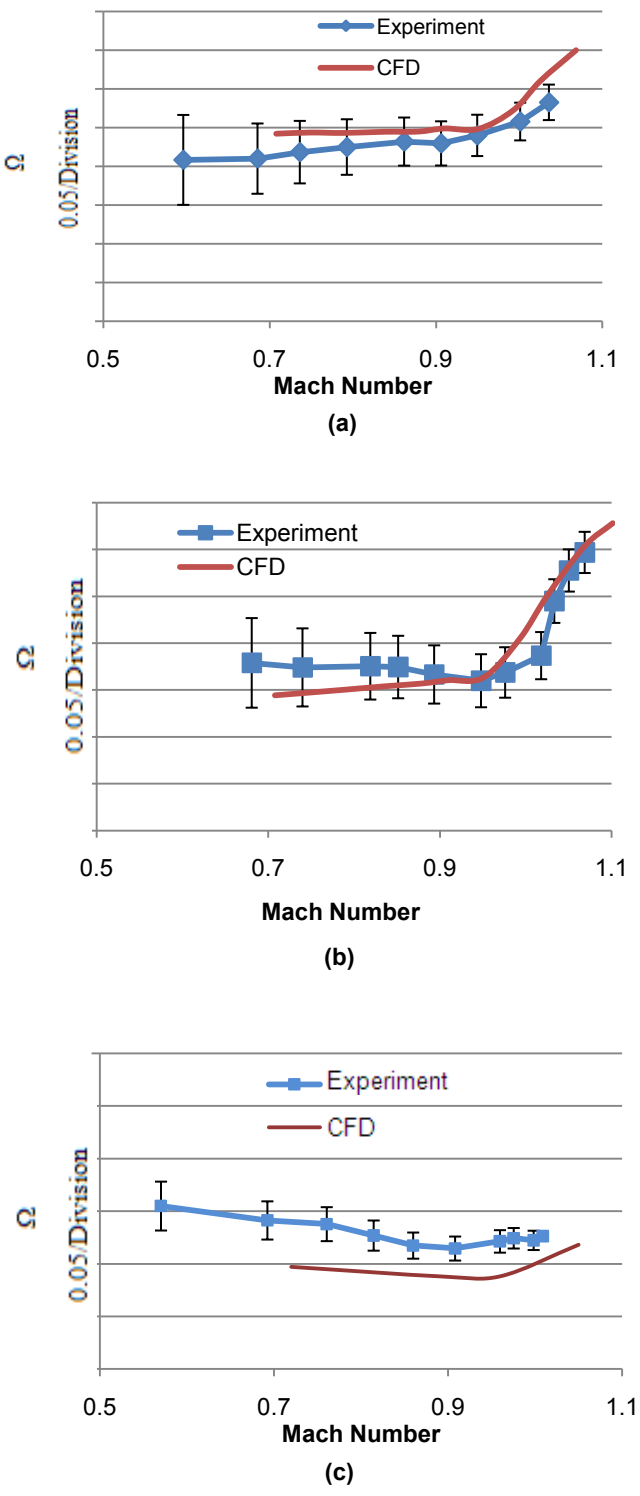

Figure 12 : Loss coefficient measurements at 1.0 axial chord downstream (a) at design incidence (b) -10 deg off design incidence (c) +10 deg off design incidence

The loss coefficient contours 0.1 axial chord downstream of the cascade show presence of strong secondary vortices contributing to high total pressure loss. CFD analysis predictions values of loss coefficient match reasonably well here but the location of secondary vortex is closer to the end

walls as compared to that observed from experimental results. Experimental results show high lift-off of the vortex core.

The loss coefficient measurements 1.0 axial chord downstream of the cascade show minimum mixed-out midspan loss coefficient for 0 incidence angle case, where as that in the case of +10 degree incidence angle is the highest due to the presence of large amount of separated flow on the suction side. Although the CFD predictions agree well with experimental measurements in general, it under predicts the losses in case of +10 degree incidence angle in particular. It was also observed that the losses rise sharply at near sonic and supersonic isentropic Mach numbers.

REFERENCES

[1] Goobie, S. M., Moustapha, S. H., and Sjolander, S. A., 1989, ‘‘An Experimental Investigation of the Effect of Incidence on the Two-Dimensional Flow,’’ Proc, IX International Symposium on Air Breathing Engines ~ISABE!, Sept., pp. 197–204.

[2] Rodger, P., Sjolander, S. A., and Moustapha, S. H., 1992, ‘‘Establishing Two- Dimensional Flow in a Large-Scale Planar Turbine Cascade,’’ AIAA Paper, No. 92-3066.

[3] Whitehouse, D. R., Moustapha, S. H., and Sjolander, S. A., 1993, ‘‘The Effects of Axial Velocity Ratio, Turbulence Intensity, Incidence, and Leading Edge Geometry on the Midspan Performance of a Turbine Cascade,’’ Can. Aeronautics Space J., 39, No. 3, Sept., pp. 150–156.

[4] Prakash, C., Cherry, D. G., Shin, H. W., Machnaim, J., Dailey, L., Beacock, R., Halstead, D., Wadia, A. R., Guillot, S., and Ng, W. F., “Effect of Loading Level and Distribution on LPT Losses,” *ASME Paper* GT2008-50052, 2008.

[5] Popovic, I., Zhu, J., Dai, W., Sjolander, S. A., Praisner, T. and Grover, E., “Aerodynamics of a Family of Three Highly Loaded Low-Pressure Turbine Airfoils: Measured Effects of Reynolds Number and Turbulence Intensity in Steady Flow”, ASME paper GT-2006-91271.

[6] Zoric, T., Popovic, I., Sjolander, S. A., Praisner, T. and Grover, E., “Comparative Investigation of Three Highly Loaded LP Turbine Airfoils: Part I – Measured Profile and Secondary Losses at Design Incidence”, ASME paper GT-2007-27537.

[7] Zoric, T., Popovic, I., Sjolander, S. A., Praisner, T. and Grover, E., “Comparative Investigation of Three Highly Loaded LP Turbine Airfoils: Part I – Measured Profile and Secondary Losses at Off-Design Incidence”, ASME paper GT- 2007-27538.

[8] Jouini, D. B. M., Sjolander, S. A., and Moustapha, S. H., 2001, “Aerodynamic Performance of a Transonic Trubine Cascade at Off-Design Conditions,” ASME J. Turbomach., 123, pp. 510–518.

[9] Jouini, D. B. M., Sjolander, S. A., and Moustapha, S. H., 2002, “Midspan Flow-Field Measurements for Two Tran-Sonic Linear Turbine Cascades at Off-Design Conditions,” ASME J. Turbomach., 124, pp. 176–186.

[10] Praisner, T. J. and Clark, J. P., “Predicting Transition in Turbomachinery, Part I – A Review and New Model Development”, ASME paper GT-2004-54108.

[11] Praisner, T. J., Grover, E. A., Rice, M. J. and Clark, J. P., “Predicting Transition in Turbomachinery, Part II – Model Validation and Benchmarking”, ASME paper GT-2004-54109.

[12] Menter, F. R., Langtry, R. B., Likki, S. R., Suzen, Y. B., Huang, P. G., “A Correlation-Based Transition Model Using Local Variables: Part I – Model Formulation”, ASME GT-2004-53452.

[13] Langtry, R. B., Menter, F. R., Likki, S. R., Suzen, Y. B., Huang, P. G., “A Correlation-Based Transition Model Using Local Variables: Part II – Test Cases and Industrial Applications”, ASME GT-2004-53454.

[14] Nagel, M. G., and Baier, R.-D., 2005, “Experimentally Verified Numerical Optimization of a Three-Dimensional Parametrized Turbine Vane With Nonaxisymmetric End Walls,” ASME J. Turbomach., 127, pp. 380–387.